Supporting Information

An [^{18}F]-positron-emitting, fluorescent, cerebrospinal fluid probe for imaging damage to the brain and spine.

Harikrishna Kommidi[1], Hua Guo[1], Nandi Chen[1,2], Dohyun Kim[3], Bin He[3], Amy P. Wu[4], Omer Aras[5*], and Richard Ting[1*]

1 Department of Radiology, Molecular Imaging Innovations Institute (MI3), Weill Cornell Medical College, New York, NY 10065, USA.

2 State Key Laboratory of Chemo/Biosensing and Chemometrics, College of Chemistry and Chemical Engineering, Key Laboratory for Bio-Nanotechnology and Molecular Engineering of Hunan Province, Hunan University, Changsha 410082, China.

3 Department of Radiology, Weill Cornell Medical College, New York, NY 10065, USA.

4 Department of Otolaryngology – Head & Neck Surgery, Northwell Health, Hofstra Northwell School of Medicine. New York, NY, 10075, USA.

5 Department of Radiology, Memorial Sloan Kettering Cancer Center, New York, NY, 10065, USA.

Co-Corresponding authors: Richard Ting, Molecular Imaging Innovations Institute (MI3), Department of Radiology, Weill Cornell Medical College, 413 East 69th Street. New York, NY 10065, USA, E-mail: rct2001@med.cornell.edu TEL: 6469626195 FAX: 6469620577 or Omer Aras, Department of Radiology, Memorial Sloan Kettering Cancer Center, New York, NY, 10065, E-mail: araso@mskcc.org. TEL: 6468884690 FAX: 6468884915

Contents

Supporting Videos.

Supporting Video S1. Dynamic imaging of an intrathecal, lumbar injection of [$^{18/19}$F]-2. Horizontal View. Video immediately prior to the acquisition of figure 2A. PET shown in red, CT in grey.

Supporting Video S2. Dynamic imaging of an intrathecal, lumbar injection of [$^{18/19}$F]-2. Sagittal View. Video immediately prior to the acquisition of figure 2A. PET shown in red, CT in grey.

Supporting Video S3. Maximum intensity projection of an iatrogenic anterior skull base CSF leak that is imaged with an intrathecal injection of [$^{18/19}$F]-2. PET shown in red, CT in grey. Video of figure 2C.

Supporting Video S4. CT of a rat bearing a puncture injury between vertebrae T7 and T8. The T7-T8 puncture injury is not visible in CT, without contrast. Video of figure 3C i-ii.

Supporting Video S5. ^{18}F-PET/CT of a rat with a puncture injury between thoracic vertebrae T7 and T8, that has been injected intrathecally, post-trauma with [$^{18/19}$F]-2. PET shown in a NIH color table. Puncture is visible with PET contrast. Video of figure 3C iv-v.

Supporting Video S6. ^{18}F-PET/CT imaging of a rat's brain ex vivo, following a traumatic event (cryolesion) to the right neocortex. The rat was injected intrathecally, post-trauma with [$^{18/19}$F]-2. PET shown in red. Brain CT in blue. Asymmetric neocortex trauma is visible with PET. Video of figure 4C iv-v.

Supporting Video S7. Confocal microscopy of the ventricle in a brain section near bregma containing [^{19}F]-2 (green). DAPI nuclear stain is shown in blue. [^{19}F]-**2** is in the ventricular space and not in the brain parenchyma. Video of figure 5E.

Supporting Video S8. CONTROL VIDEO. Attempts at SPECT imaging equicurie quantities (100 µCi) of intrathecal [^{99m}Tc]-DTPA failed to produce high resolution images of the intrathecal space. [^{99m}Tc]-DTPA was injected intrathecally and imaged by SPECT/CT on an Inveon SPECT/CT (Imaging at 20 min post injection, 10 min CT, followed by 30 min single pinhole SPECT acquisition. The kidneys and bladder are clearly visible, but unlike in supporting videos S1 through S6, activity in the intrathecal space is not clearly resolved. Video of supporting figure S14E.

1. **Synthetic Chemistry:**

The following synthesis of a fluorescein-bearing methyl ammonium trifluoroborate **2** was performed:

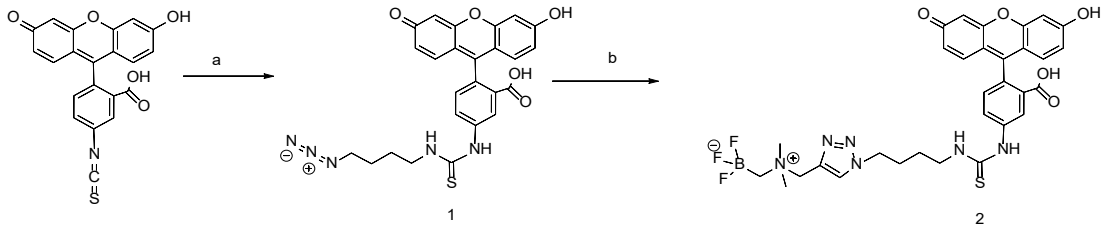

Scheme S1. Reagent and conditions: (a) 1.2 eq 4-Azidobutan-1-amine, DMF, RT, 12h; (b) N,N-Dimethyl-N-Propargyl-N-Methyl trifluoro borate, 1.0M $CuSO_4$ 4.5 H_2O, 1.0 M Sodium ascorbate, DMF, 50°C, 6 hours.

1.1. General synthetic methods

Chemicals were purchased from Oakwood Chemical, Aldrich, Combi-blocks, or Alfa Aesar. Fluorescein (F2456) and Fluorescein isothiocyanate isomer I (F4274) were purchased from Aldrich. Sterile, endotoxin and mycoplasma free, isotonic, 1x PBS was purchased from (pH 7.4 ± 0.1, Corning Cellgro 21-040-CM). Analytical, reverse phase UPLC-MS were performed on a Waters Acquity H class HPLC/ SQD2 mass spectrometer and a Phenomenex Kinetex 1.7µm C18 100Å, 50 cm x 2.1 mm I.D. column (00B-4475-AN), with a 1.5 min, a10-90% H_2O:acetonitrile (ACN) (0.05% TFA) gradient and a flow rate of 0.6 mL/min (unless stated otherwise). Preparative HPLC was performed on a Agilent 1200 Series HPLC equipped on a Phenomenex Luna C18(2) 100Å, 250 cm x 21.20 mm I.D. 10 µm reverse phase column (00G-4253-P0 AX), with a 20 min, a10-90% H_2O:ACN (0.05% TFA) gradient and a flow rate of 15 mL/min. ^{1}H, ^{13}C, and ^{19}F-NMR were performed on a 500 MHz Bruker spectrometer. Thermo Scientific 5 mL Reacti-Vial #13223 were used for fluoride concentration.

1.2. Characterization of 1-(4-azidobutyl)-3-(6'-hydroxy-3,3'-dioxo-3',9a'-dihydro-3*H*-spiro[isobenzofuran-1,9'-xanthen]-6-yl)thiourea (**1**)

1.2.1. ^{1}H NMR (DMSO-d6, 500 MHz, 21 °C):

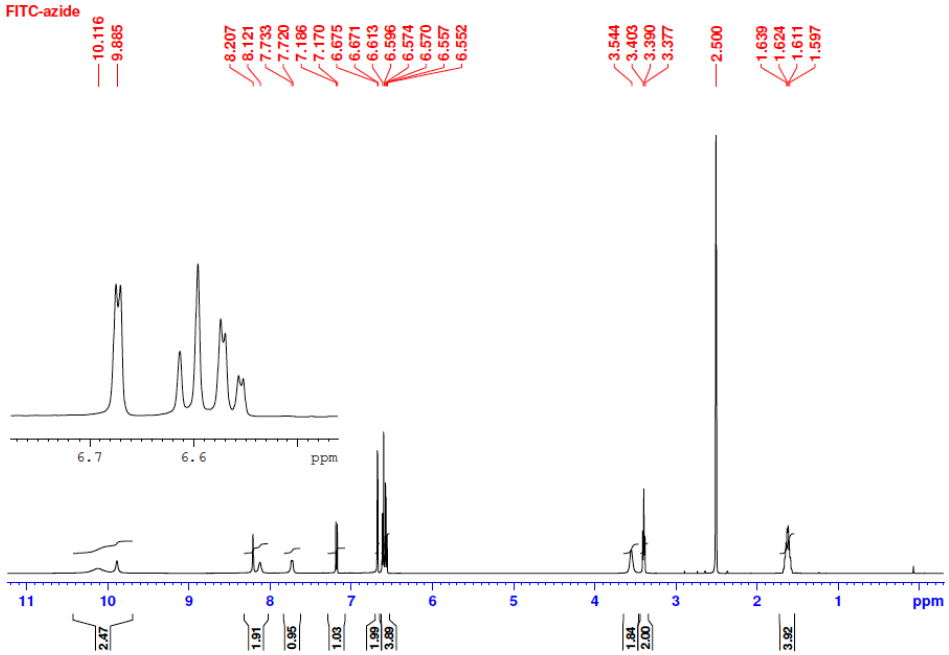

1.2.2. ^{13}C NMR (DMSO-d6, 500 MHz, 21 °C):

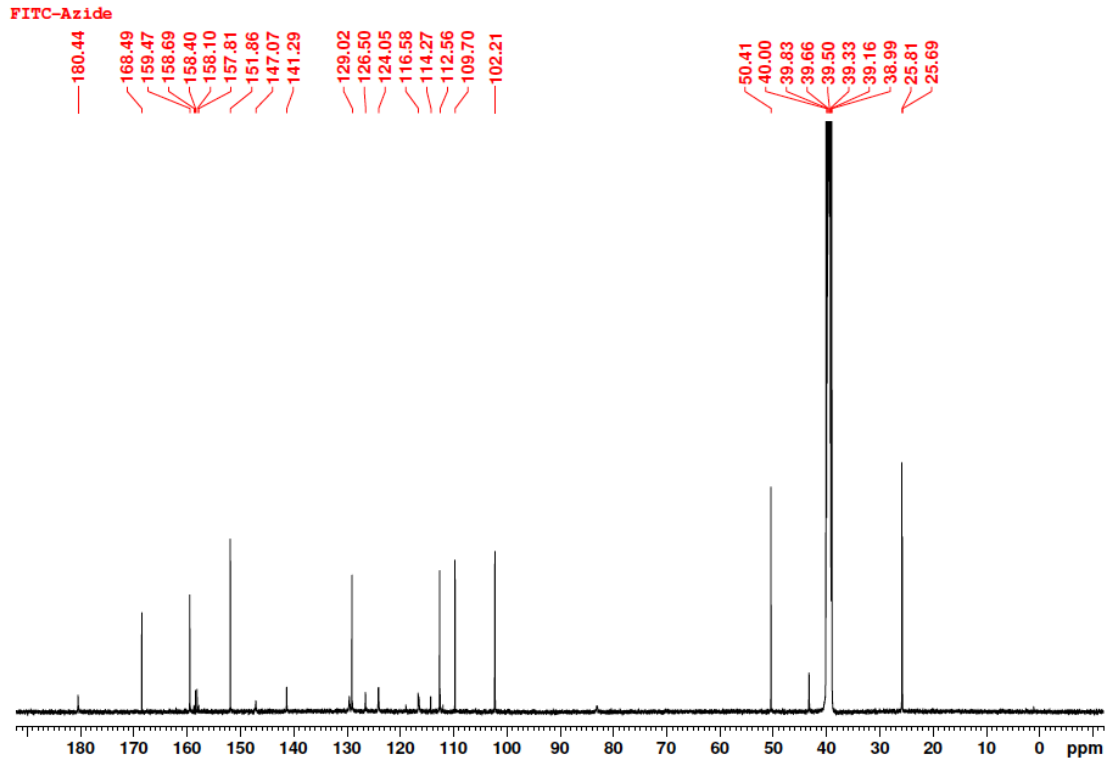

1.2.3. UPLC-MS^+:

a10-90% H_2O:ACN (0.05% TFA), 1.5 min gradient, 0.6 mL/min flow, det. 1441 M/Z, 215, 450, nm Abs spectra. Elution time: 1.33 min.

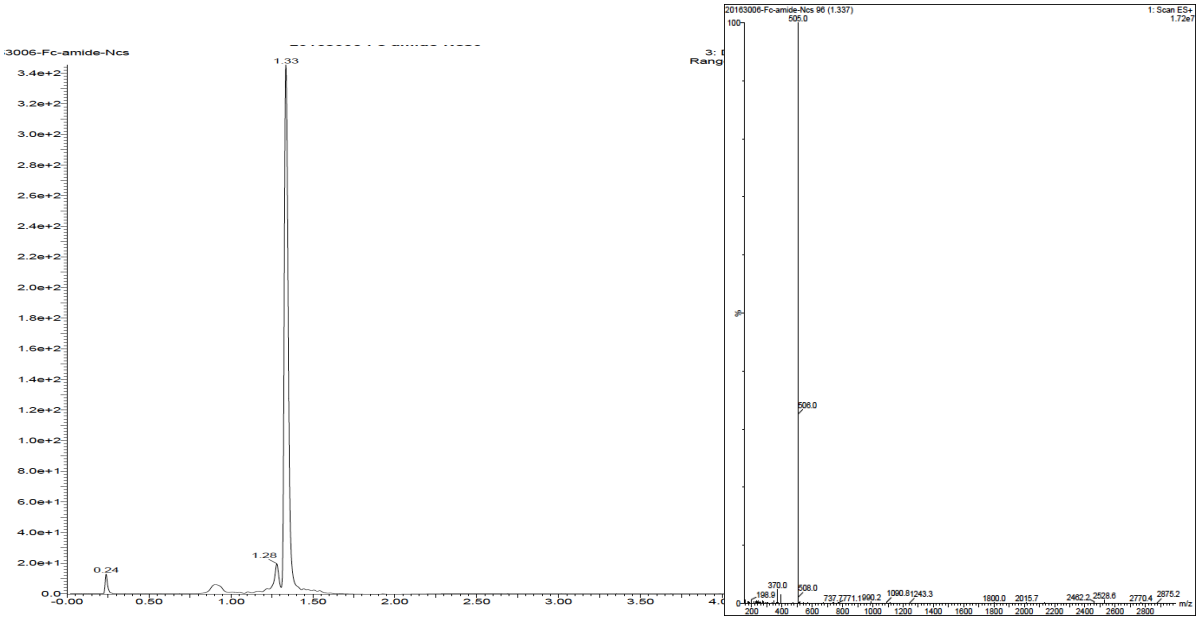

1.2.4. HRMS:

Agilent HMS 6550 QToF. Methanol. m/z calculated for $C_{25}H_{21}N_5O_5S$ $[M + H]^+$: 504.1336, found: 504.1336.

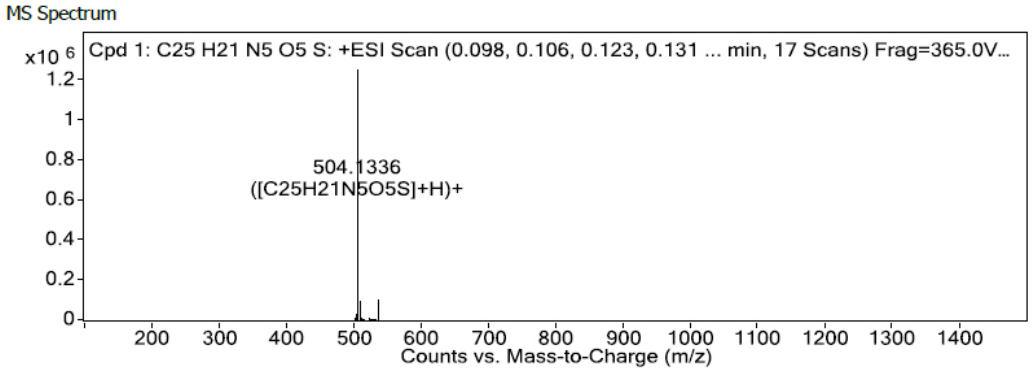

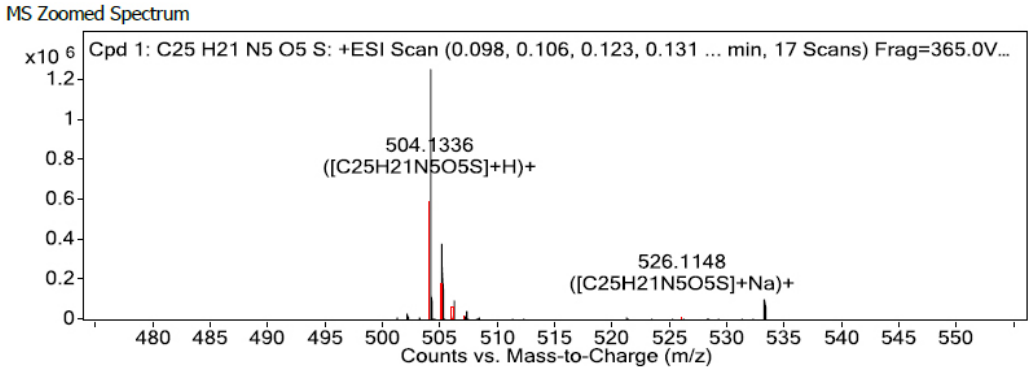

1.3. Trifluoro((((1-(4-(3-(6'-hydroxy-3,3'-dioxo-3',9a'-dihydro-3*H*-spiro[isobenzofuran-1,9'-xanthen]-6-yl)thioureido)butyl)-1*H*-1,2,3-triazol-4-yl)methyl)dimethylammonio)methyl)borate (**2**):

1.3.1. ^{1}H NMR (DMSO-d6, 500 MHz, 21 °C):

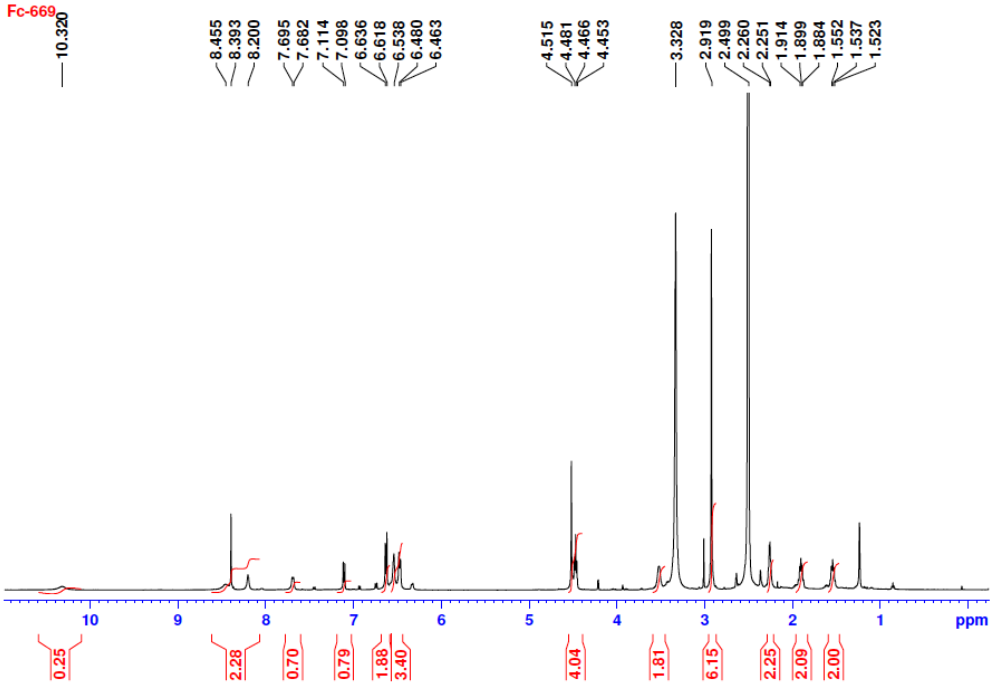

1.3.2. ^{13}C NMR (DMSO-d6, 500 MHz, 21 °C):

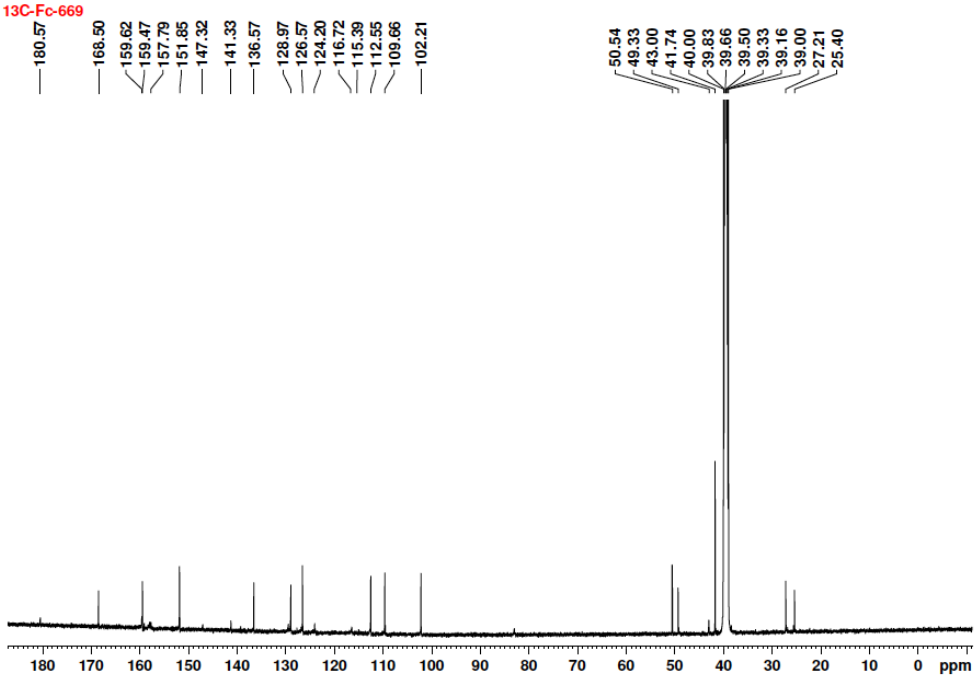

1.3.3. ^{19}F NMR (1x PBS pH 7.4, 500 MHz, 21 °C):
CF_2Cl_2 (0 ppm), trifluoracetic acid standard (-78 ppm)

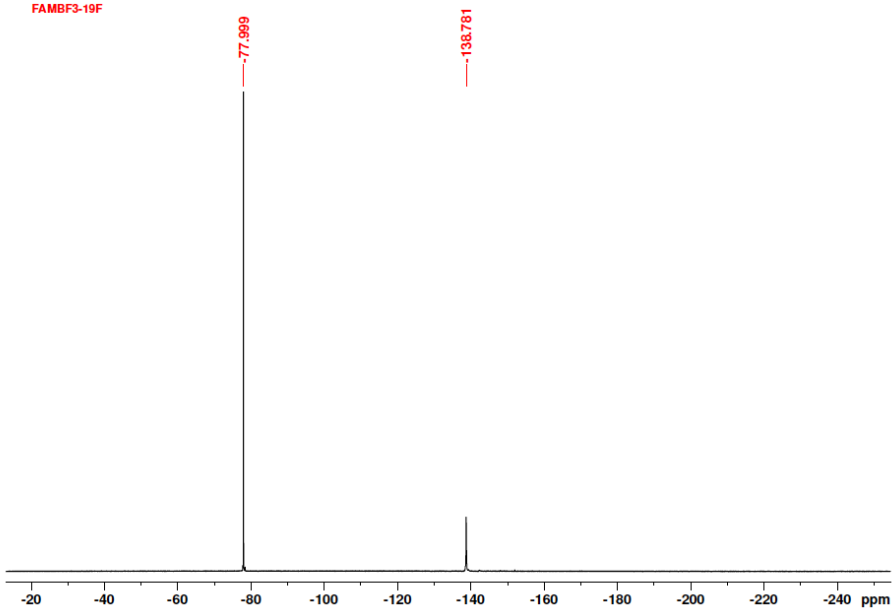

1.3.4. UPLC-MS^+:
a10-90% H_2O:ACN (0.05% TFA), 1.5 min gradient, 0.6 mL/min flow, det. 1441 M/Z, 215, 450, nm Abs spectra. Elution time: 1.17 min.

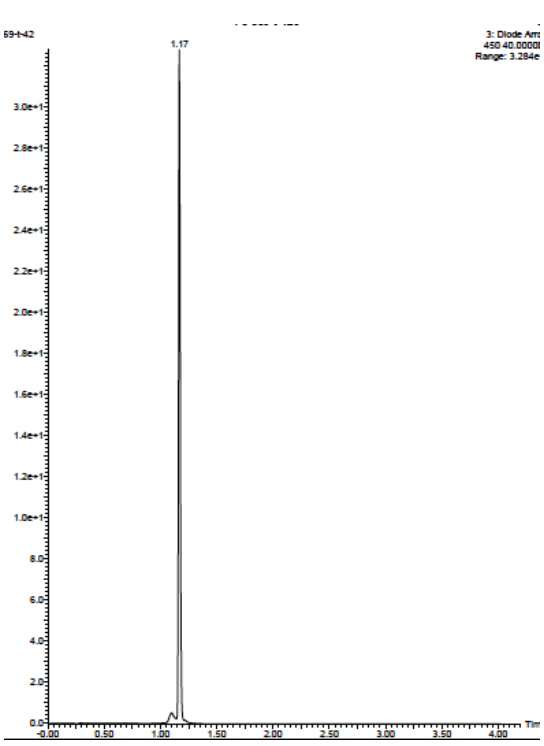

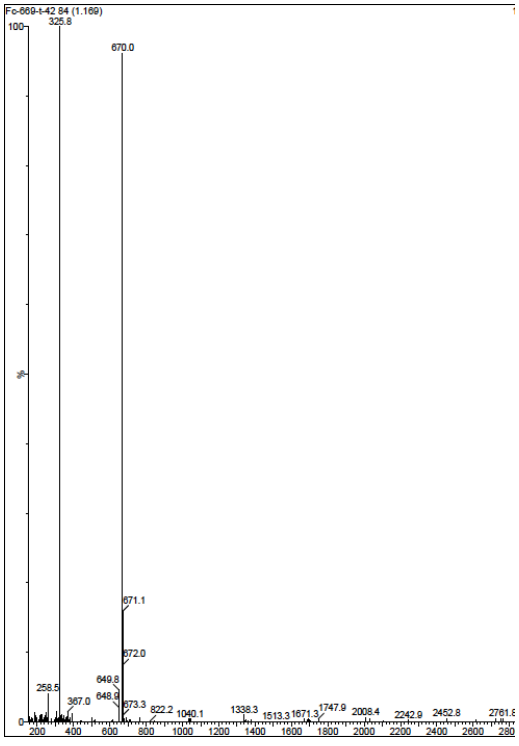

1.3.5. HRMS:

Agilent HMS 6550 QToF. Methanol. m/z calculated for $C_{31}H_{32}NBF_3N_6O_5S + H^+$ $[M + H]^+$: 669.2278, found: 669.2281.

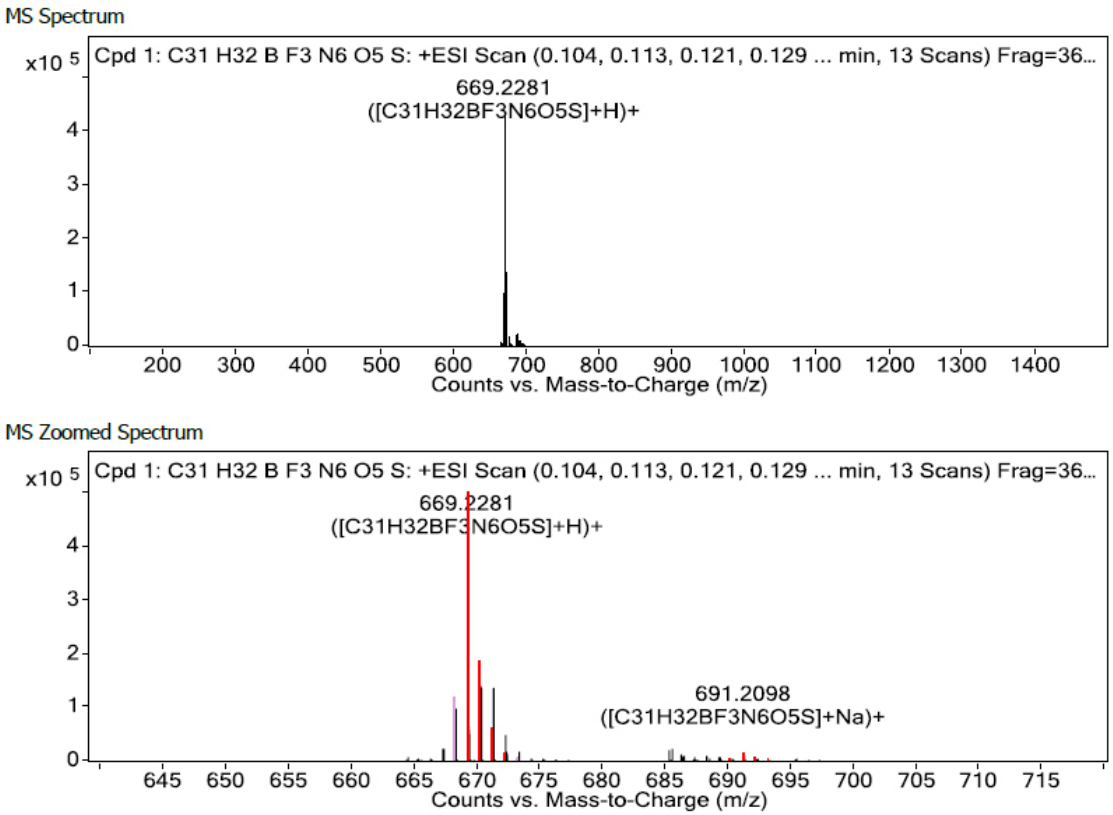

2. **Fluorescence properties of 2.**

For **2** to serve as a multimodality analogue of fluorescein, the fluorescence properties of the two compounds must be similar. The Normalized excitation and emission spectra of **2** and fluorescein (reference), reported in table 1, taken in PBS and 10mM NaOH-Ethanol, are shown below:

2.1. Fluorescence Spectrum of fluorescein dye in PBS

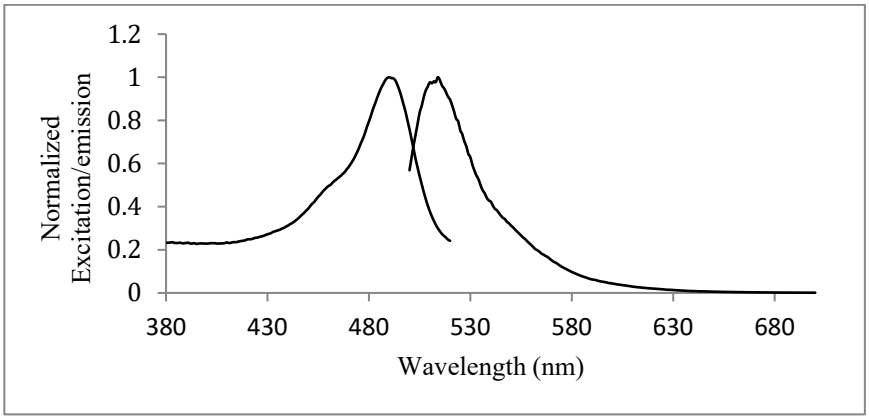

2.2. Fluorescence Spectrum of fluorescein dye in 10mM NaOH-EtOH

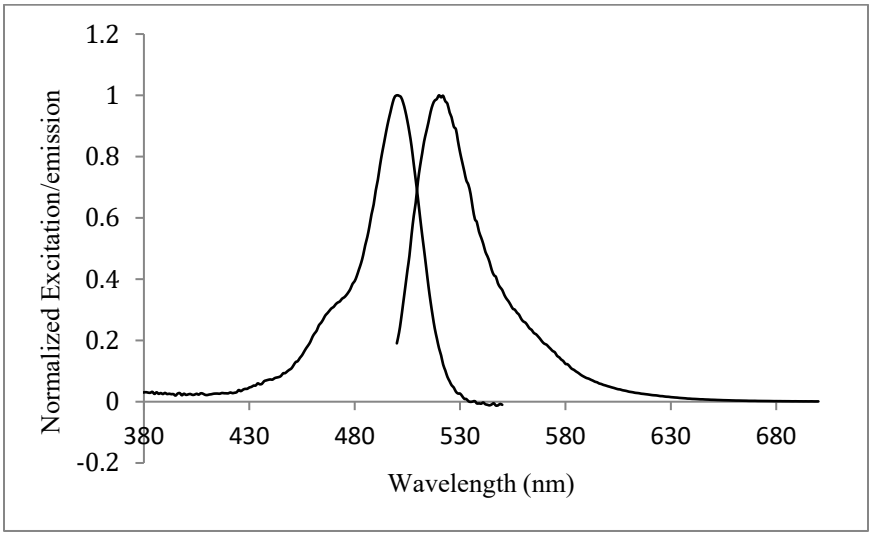

2.3. Fluorescence Spectrum of **2** in PBS

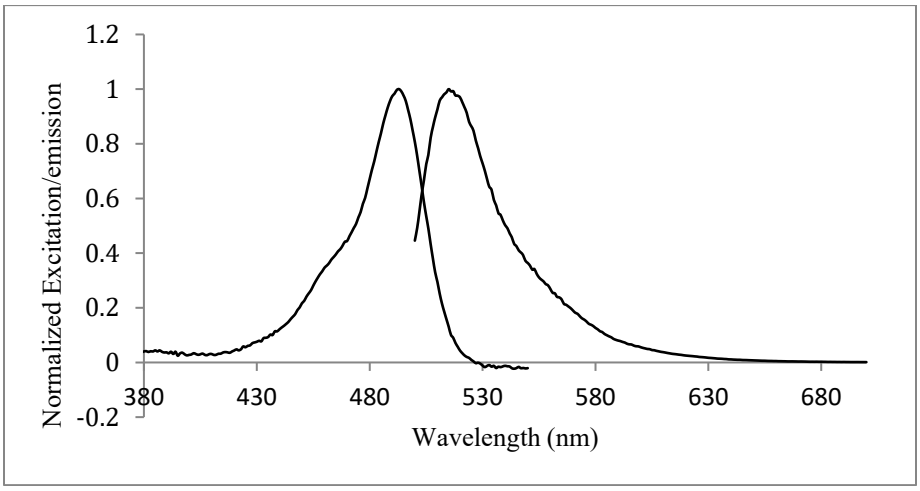

2.4. Fluorescence Spectrum of **2** in 10mM NaOH-EtOH

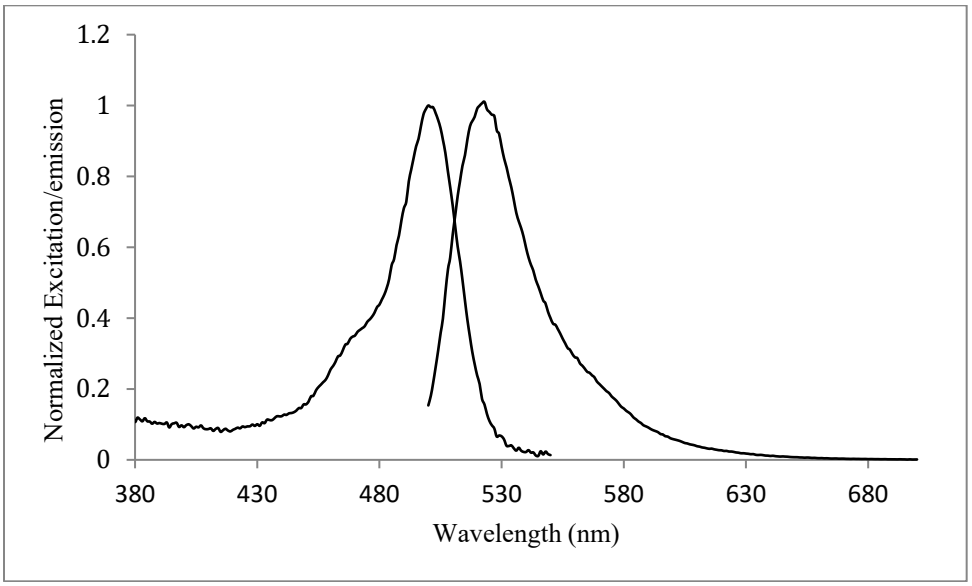

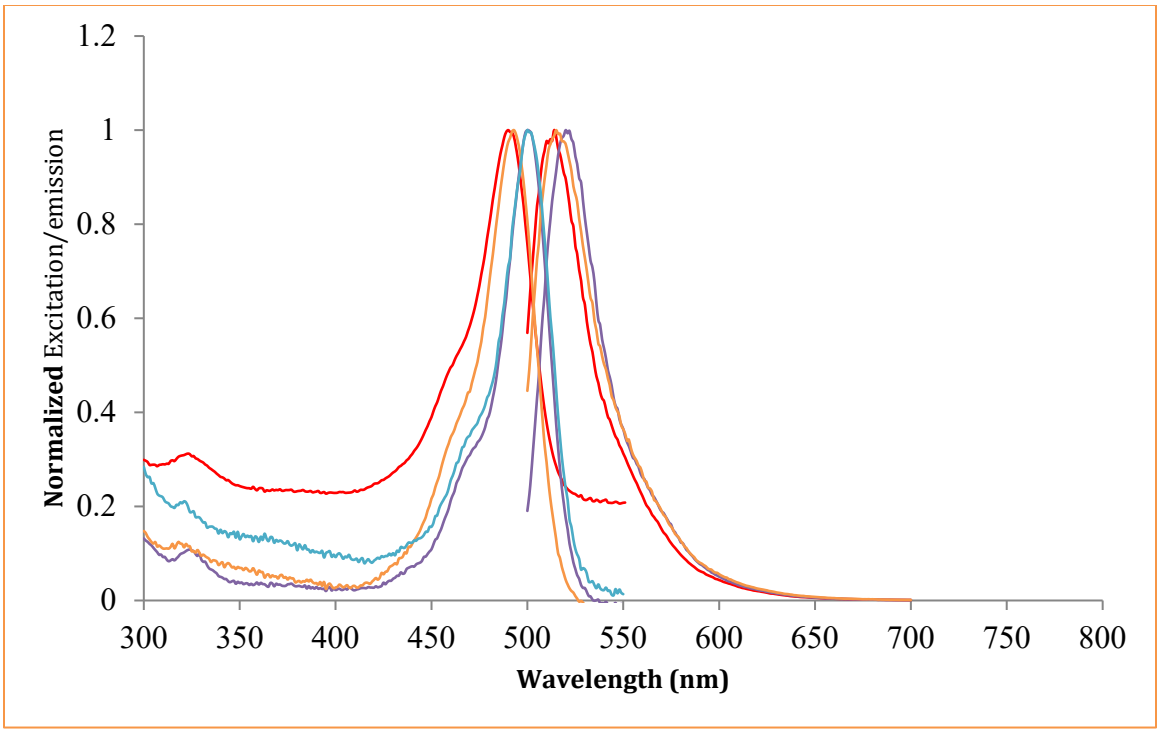

Fluorescein in 1x PBS Ex $_{490\ nm}$ 5 and 5 slits ex/em
Fluorescein in 10mM NaOH-EtOH Ex $_{490\ nm}$ 5 and 5 slits ex/em
2 in1x PBS Ex $_{490\ nm}$ 5 and 5 slits ex/em
2 in 10mM NaOH-EtOH Ex $_{490\ nm}$ 5 and 5 slits ex/em

Supporting figure S1. Plot of normalized absorbance and emission spectra of fluorescein and 2 in PBS and in 10mM NaOH EtOH. The excitation and emission spectra for **2** and fluorescein at pH 7.4 and in strong base are shown on the same graph.

2.5. Absorbance spectroscopy properties of **2**.

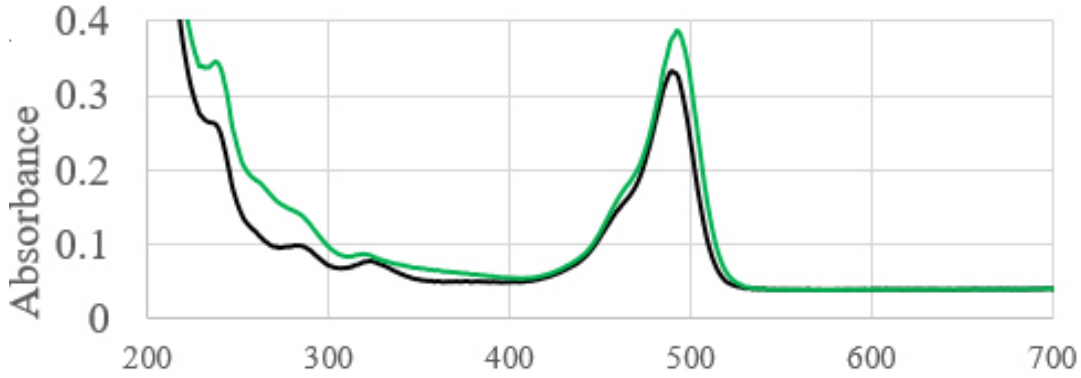

Supporting figure S2. Absorbance spectra of 5 µM solutions of fluorescein (black) and [$^{18/19}$F]-2 (green) in 1x PBS, pH 7.4, measured on a Cary 60 absorbance spectrometer.

3. **Trifluoroborate/ester stability in physiological pH**

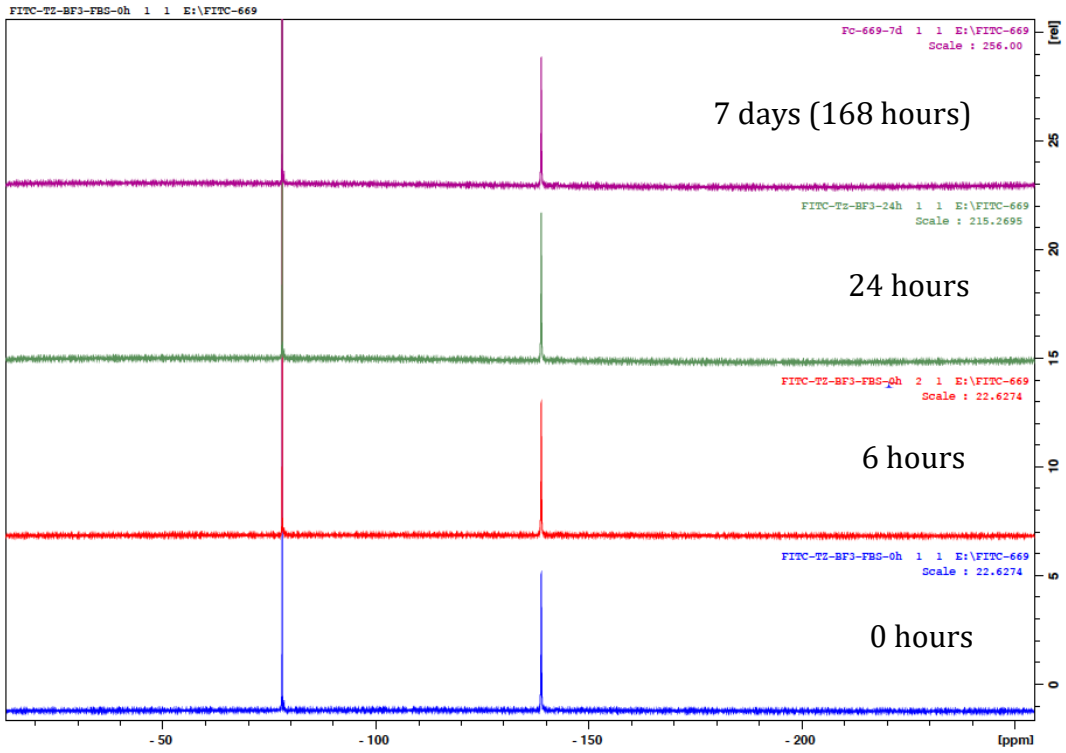

Supporting Figure S3. Stability assay in DMSO-1x PBS demonstrating that 2 does not lose fluoride at physiological pH. Ideally, a fluoride labeled compound should be stable *in vivo*. We performed an *in vitro* test as described by Perrin[25-26], to show that **2** is stable at physiological pH. **2** was placed in 50% DMSO-d6: 1x PBS solution (1:1) at pH = 7.4. Daily ^{19}F-NMR is used to follow boron-fluoride bond hydrolysis. The presence of fluoride ion was not observed after 7 days of incubation at 21°C ($t_{1/2}$ defluoridation >7 days). No change in the ^{19}F-NMR spectra is observed. Free fluoride ion is not observed (from defluoridation) suggesting that **2** is stable.

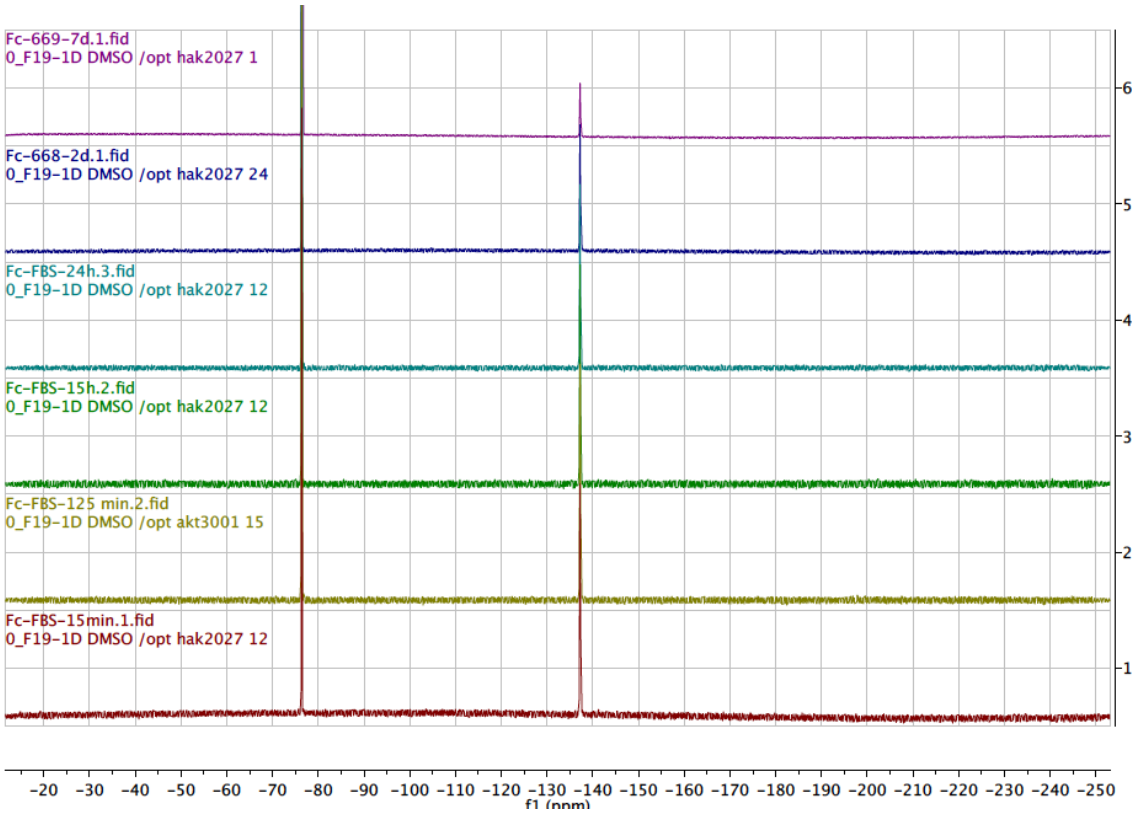

Supporting Figure S4. Stability assay in DMSO-FBS demonstrating that 2 does not lose fluoride under physiological conditions. [^{19}**F**]**-2** was placed in 50% DMSO-d6: 1x FBS solution (1:1) Daily ^{19}F-NMR was used to follow boron-fluoride bond hydrolysis. The presence of fluoride ion was not observed after 7 days of incubation at 21°C ($t_{1/2}$ defluoridation >7 days).

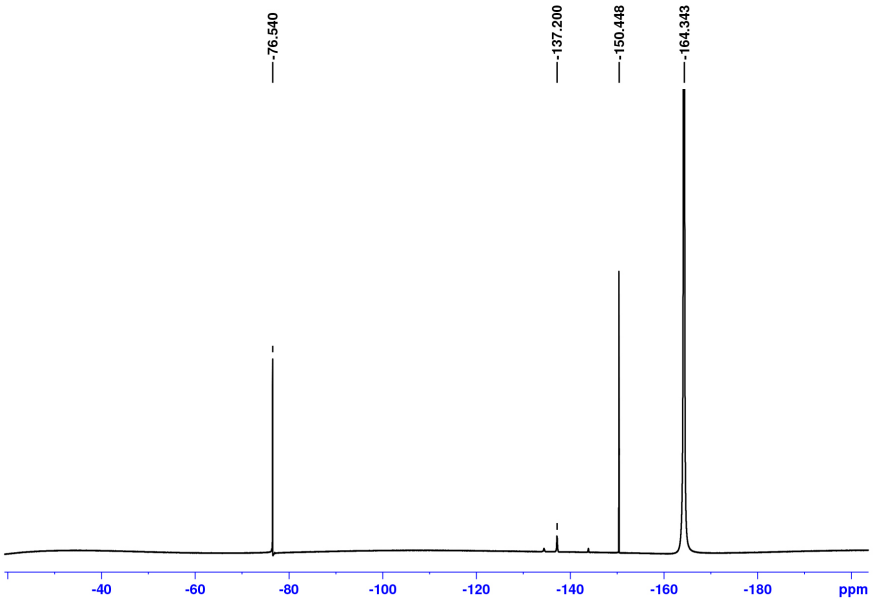

Supporting figure S5. ^{19}F-NMR Spectra of 2 in DMSO-FBS in the presence of a ^{19}F- sodium fluoride spike. To a solution of [^{19}F]**-2** incubated in 50% DMSO-d6: 1x FBS solution (1:1) for 7 days (-137.2 ppm), sodium fluoride was added. Two new shifts corresponding to fluoride ion in a NMR tube are observed (-150.5 and -164.3 ppm). If [^{19}F]**-2** were to defluoridate in supporting figures S3 and S4, fluoride NMR spectrum would resemble this control experiment.

Date	Initial Volume of **[^{19}F]-2** in DMSO (8 mM)	Activity of ^{18}F-fluoride ion precursor at time of addition to **[^{19}F]-2**	Quantity of **[^{19}F]-2** (nmol)	Volume 1.0 M Pyridazine-HCl pH= 2.5	Isolated activity of **[^{19}F]-2**	Total time of synthesis (Rxn and purification)	Decay uncorrected Radio chemical yield	Specific activity assuming 60% yield of **[^{18}F]-2** (Ci/µmol)
03/032017	10µL	24 mCi	80	10µL	2.50 mCi	1h	10.41%	0.031
02/28/2017	10µL	30 mCi	80	10µL	4.60 mCi	55 min	15.33%	0.095
02/21/2017	10µL	35 mCi	90	10µL	4.50 mCi	1h 15 min	12.85%	0.083
01/10/2017	10µL	20 mCi	89	10µL	2.50 mCi	50 min	12.50%	0.047
11/11/2016	10µL	5.6 mCi	160	10µL	1.63 mCi	50 min	29.10%	0.016
11/02/2016	10µL	6.1 mCi	160	10µL	1.65 mCi	50 min	27.30%	0.017
10/27/2016	10µL	7.1 mCi	160	10µL	0.95 mCi	50 min	13.30%	0.010
10/24/2016	10µL	1.0 mCi	80	10µL	0.195 mCi	50 min	19.5%	0.004

Supporting figure S6. Radiochemical syntheses. Yield and reactivity data from multiple labelings of [^{18}F]-2. Radio chemical labeling experiments were carried out on ^{19}F-**2**, following the protocol described in the materials and method.

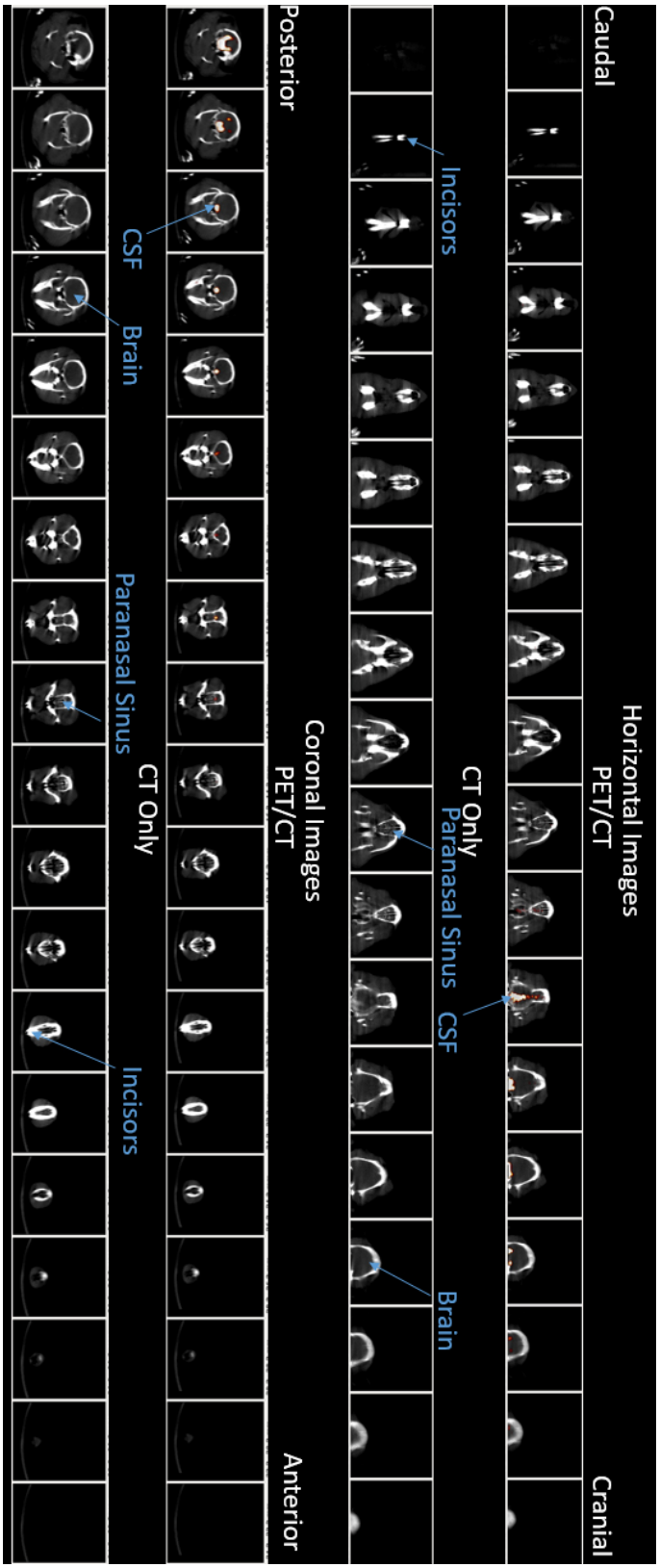

Supporting figure S7. Axial and horizontal cross-sectional analyses of figure 2A (pre-trauma imaging). PET/CT and CT-only cross sections (2 mm) of rat in figure 2A. Pre-trauma imaging shows no [$^{18/19}$F]-**2** (activity) in the paranasal sinus following intrathecal injection.

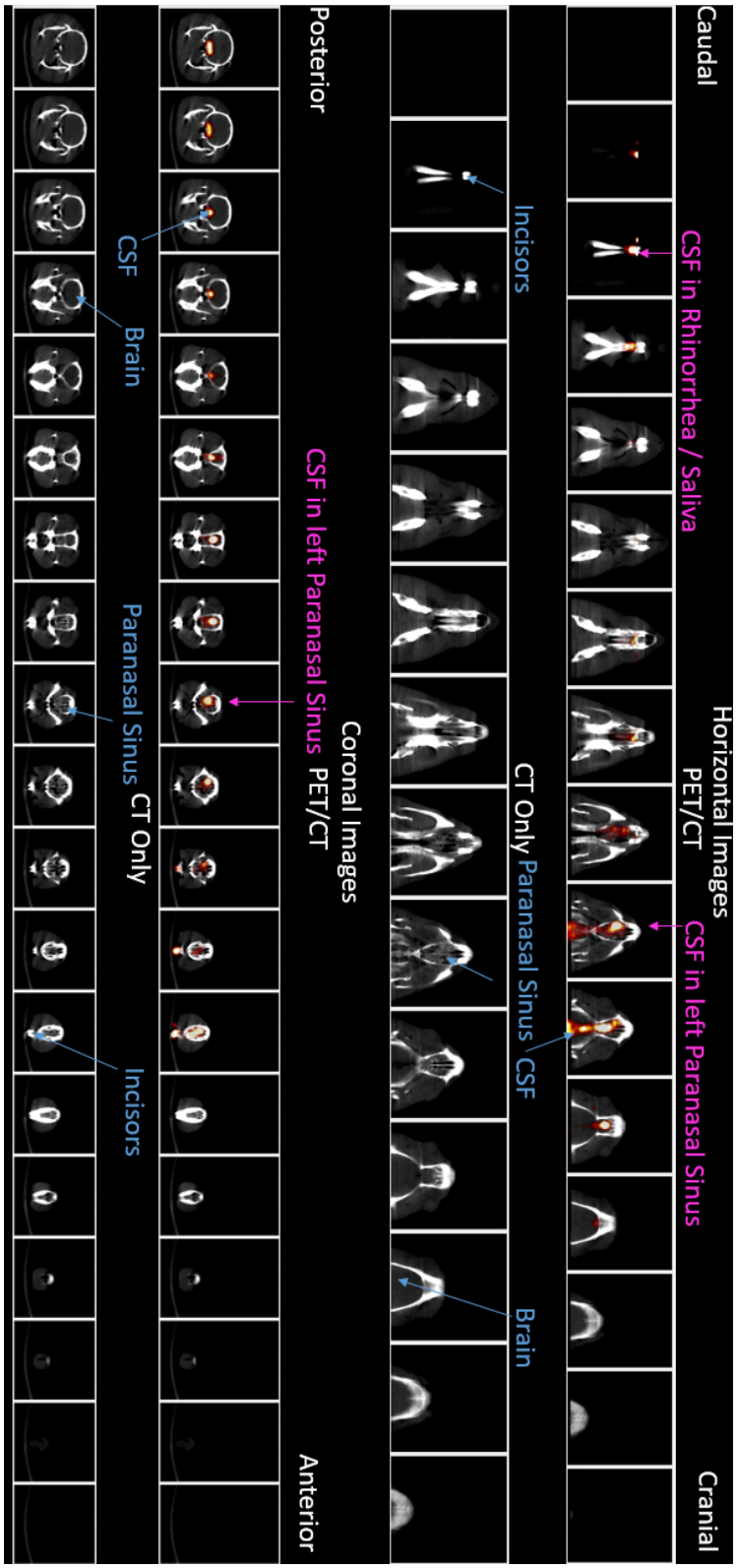

Supporting figure S8. Axial and horizontal cross-sectional analyses of figure 2C (post-trauma imaging). PET/CT and CT-only cross sections (2 mm) of rat in figure 2C. Post traumatic imaging shows [$^{18/19}$F]-**2** (activity) **only** in the left paranasal sinus following intrathecal injection and trauma.

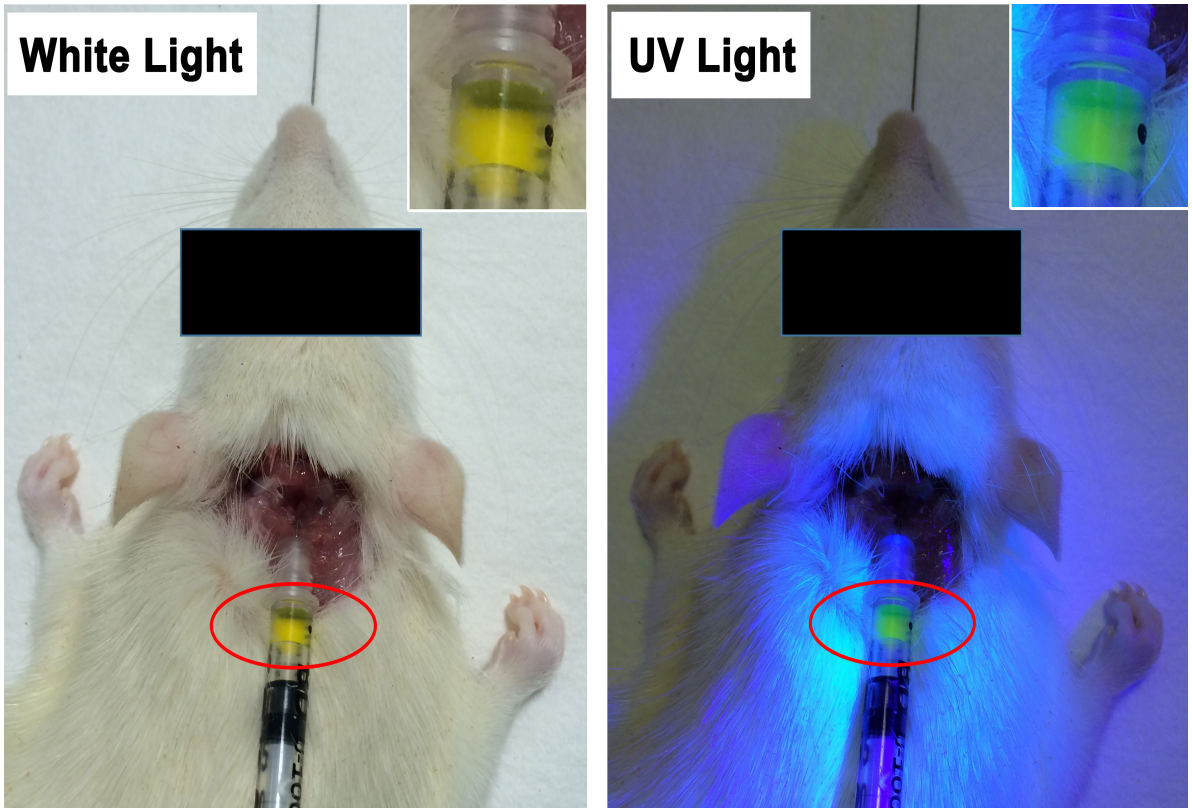

Supporting figure S9. [$^{18/19}$F]-2 injected through the lumbar spine can be collected in the CSF of the cisterna magna. Proper collection of the CSF from the cisterna magna results in a straw-colored fluid (CSF) that is free of blood. This fluid is fluorescent under a hand-held, LED blacklight in rats that bear an intrathecal dose of [$^{18/19}$F]-**2**.

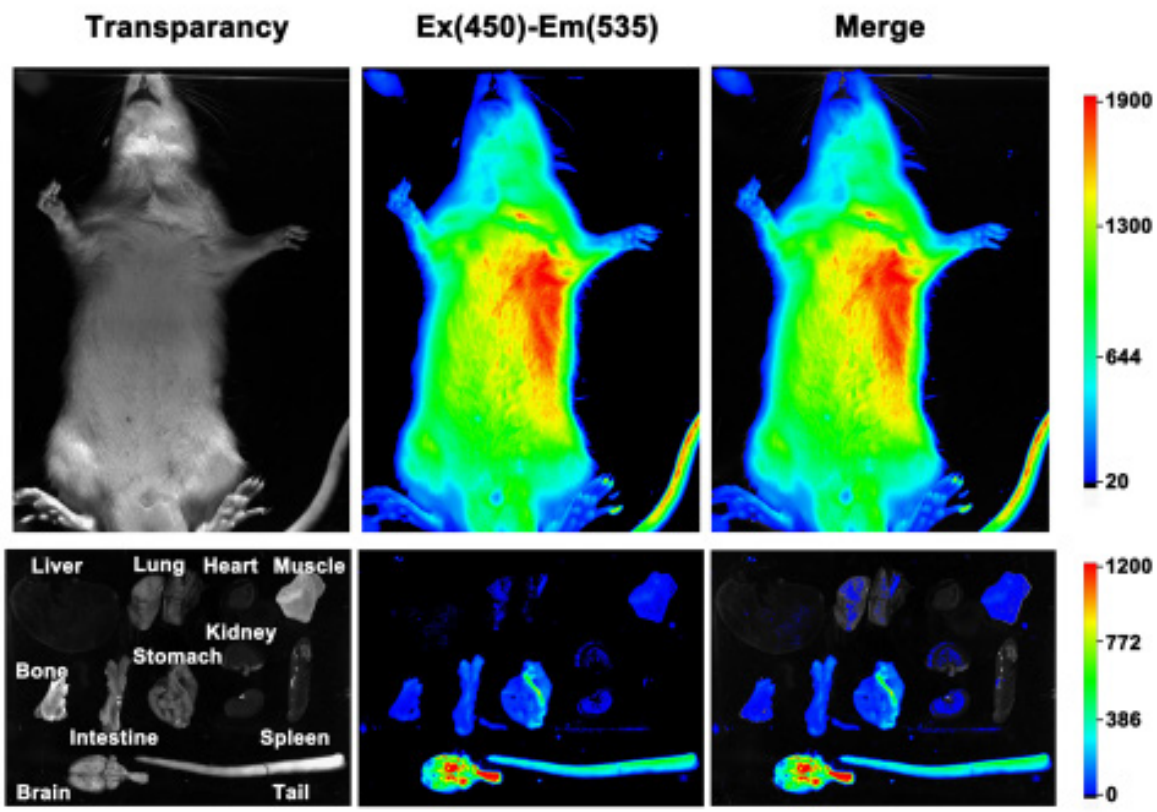

Supporting figure S10. In vivo and ex vivo fluorescent analysis of a rat bearing intrathecally injected [$^{18/19}$F]-2. Fluorescent imaging on a Bruker extreme cannot be used to visualize intrathecal [$^{18/19}$F]-**2** through the skin, fur, vertebrae, and skull of a rat. Ex vivo analysis of organs show intrathecal [$^{18/19}$F]-**2** in the brain and stomach as expected from biodistribution (Figure 6A).

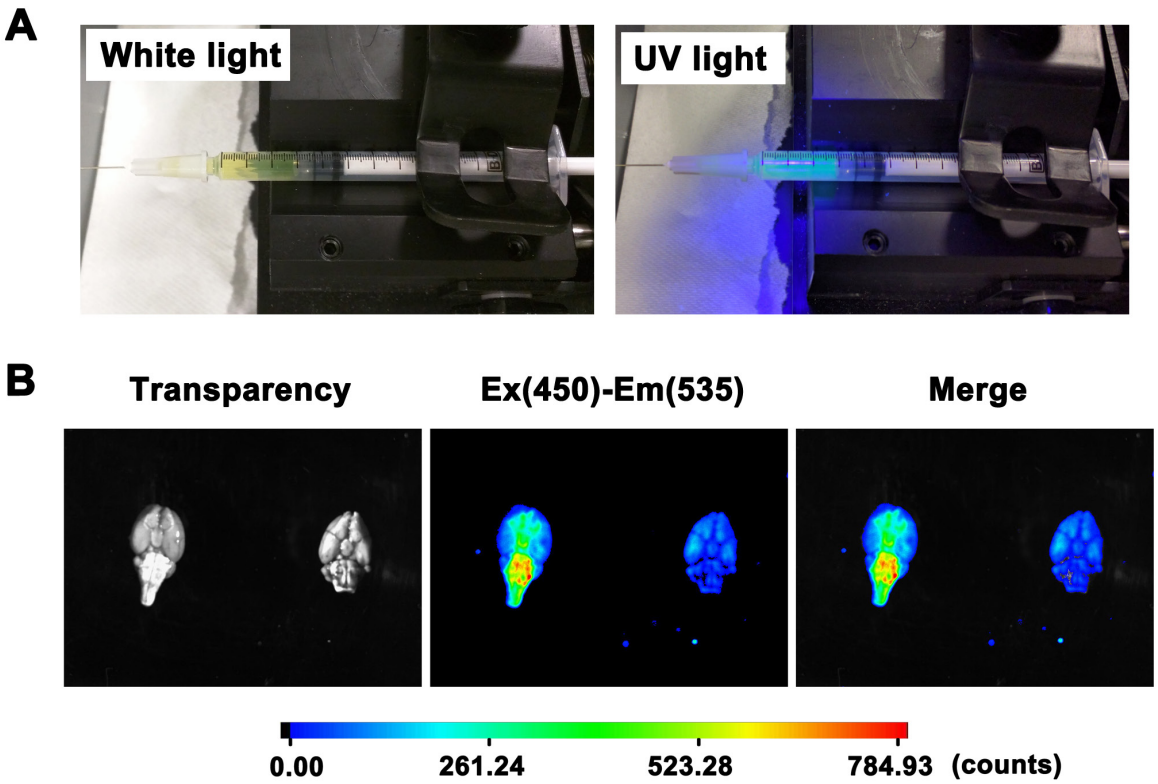

Supporting figure S11. [$^{18/19}$F]-2 is highly fluorescent, and the cisterna magna and ventricles of a rat only become fluorescent in the presence of [$^{18/19}$F]-2. (A) A syringe filled with [$^{18/19}$F]-**2**, ready for intrathecal injection, is fluorescent when lit with a LED blacklight. (B) As a control, a brain from a rat without contrast was imaged alongside a rat's brain with [$^{18/19}$F]-**2**. Only the CSF space (i.e. the ventricles and the cisterna magna) of the brain of the rat bearing [$^{18/19}$F]-**2** are visible under fluorescent conditions. Ventral view is shown.

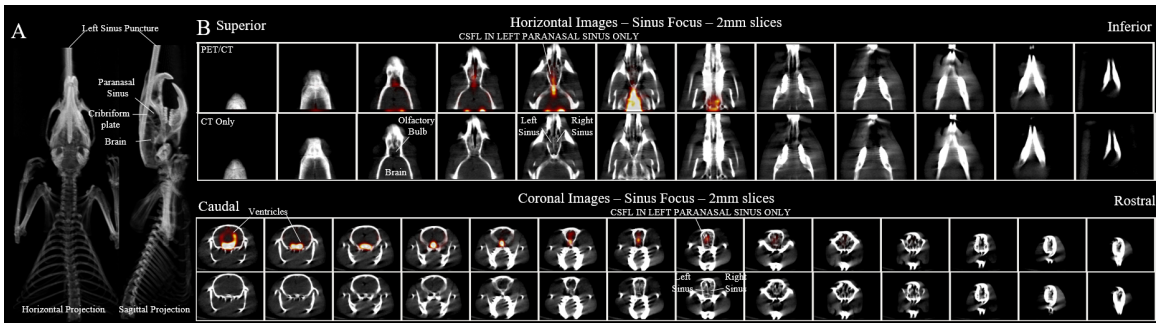

Supporting figure S12. Trauma model #1. Iatrogenic anterior skull base CSF leak REPLICATE NUMBER 2. (A) Mid-trauma CT image showing trauma to the left cribriform plate leading to CSFL in the left paranasal sinus. Trauma is induced with a 25G needle (0.5144 ±0.0064 mm) that is passed through the left nostril to pierce the cribriform plate to induce CSF leakage from the olfactory bulb into the paranasal sinus. (B) Post trauma imaging of intrathecally injected [$^{18/19}$F]-**2**. PET/CT and CT-only cross sections (2 mm) of the rat show [$^{18/19}$F]-**2** activity in the left paranasal sinus. Right side CSFL is not observed. Note that PET (15 min)/CT (10 min) imaging was performed with the intact needle, i.e. the needle still occludes the leak, so the area of the CSF tear (and the volume from which CSF can leak) is significantly less than the outer diameter of the needle (0.5144 ±0.0064 mm). A smaller needle was used (25G vs. 22G, so trauma is less obvious).

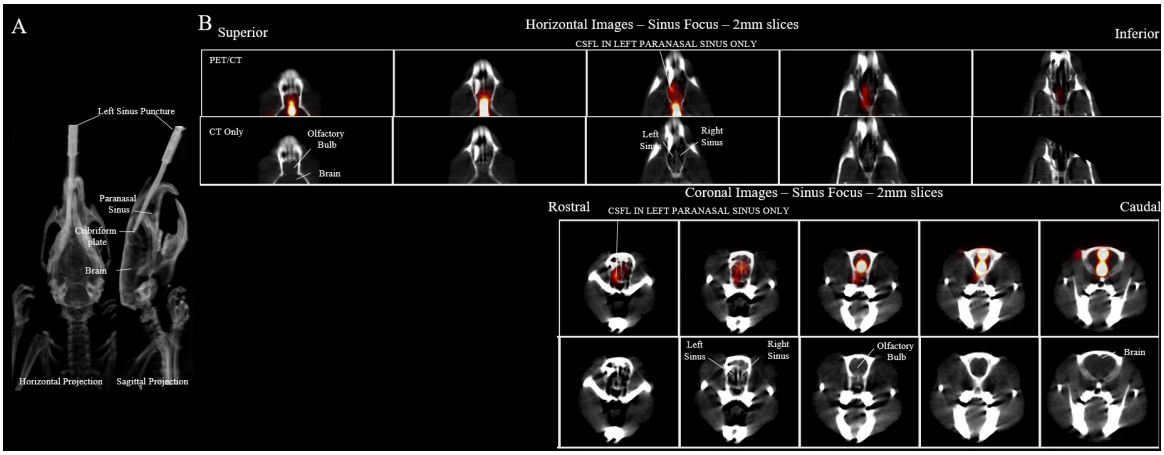

Supporting figure S13. Trauma model #1. Iatrogenic anterior skull base CSF leak REPLICATE NUMBER 3. (A) Mid-trauma CT image showing trauma to the left cribriform plate leading to CSFL in the left paranasal sinus. Trauma is induced with a 22G needle (0.7176 ±0.0064 mm) that is passed through the left nostril to pierce the cribriform plate to induce CSF leakage from the olfactory bulb into the paranasal sinus. Based on CT imaging from the previous two rats, the needle length has been reduced (2.5 cm) so that the needle pierces the cribriform plate and olfactory bulb, generating CSFL, but does not pass into the neocortex (which could unnecessary cause morbidity or mortality in live rats). (B) Post trauma imaging of intrathecally injected [$^{18/19}$F]-**2**. PET/CT and CT-only cross sections (2 mm) of the rat show [$^{18/19}$F]-**2** activity in the left paranasal sinus. Right side paranasal sinus [$^{18/19}$F]-**2** activity is not observed. Note that PET (15 min)/CT (10 min) imaging was performed with the intact needle, i.e. the needle is occluding the leak, so the area of the CSF tear (and the area from which CSF can leak) is significantly less than the outer diameter of the needle (0.7176 ±0.0064 mm).

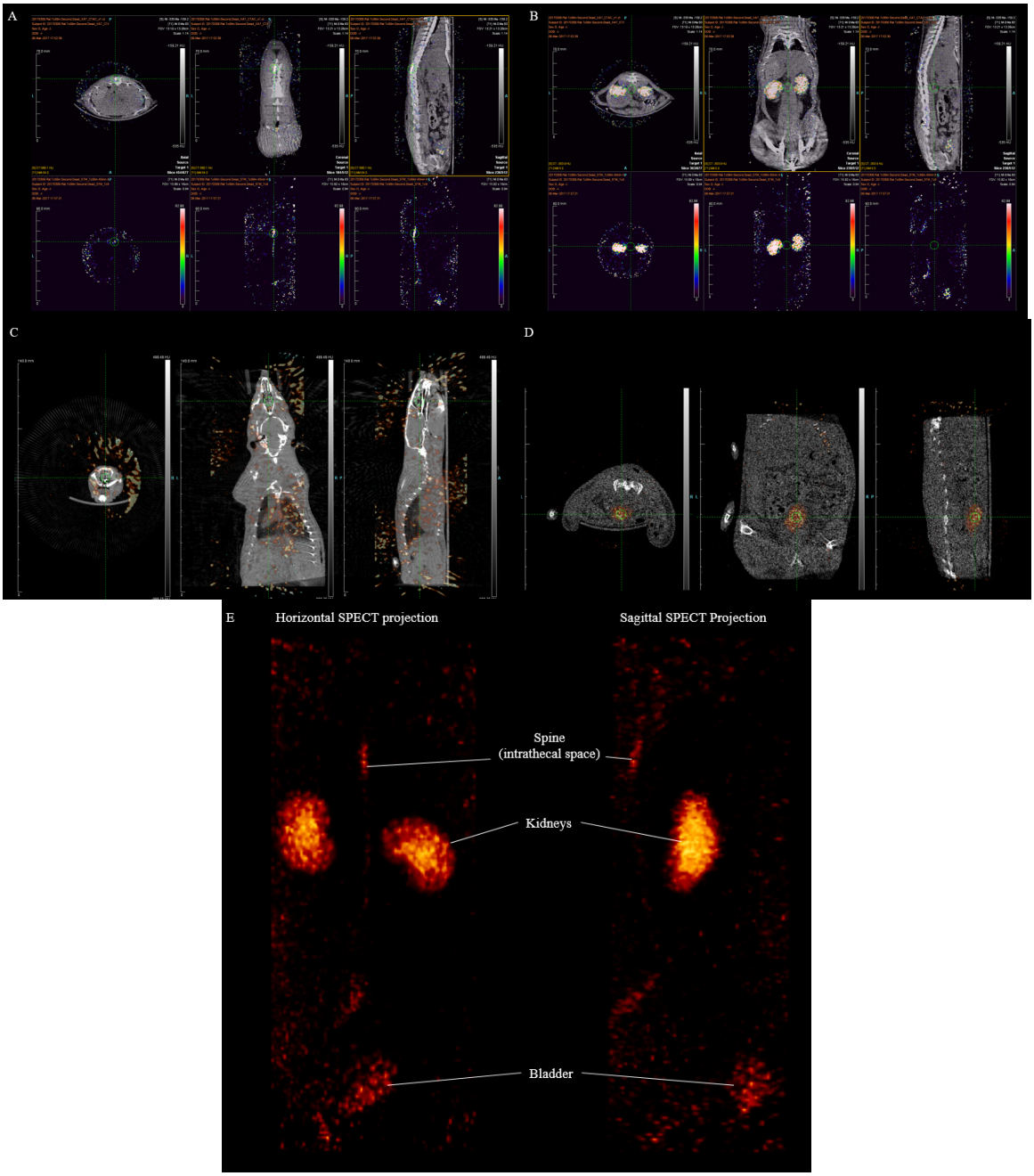

Supporting figure S14. SPECT attempts to image an iatrogenic anterior skull base CSF leak using [^{99m}Tc]-DTPA. An intrathecal catheter was implanted into a rat (L5-L6). Its presence in the intrathecal space was confirmed by the observation of a tail-flick response. Following implantation of the catheter, an iatrogenic CSF leak was created using 22G needle. Immediately following leak generation, 100 µCi of [^{99m}Tc]-DTPA was injected through the intrathecal catheter. The 22G needle was withdrawn from the nasal sinus and blood filled rhinorrhea from the left nostril was surveyed for radioactivity. Activity in rhinorrhea was confirmed. This survey took 20 min. Upon the confirming of activity in the nasal drainage, the rat was transferred to an Inveon SPECT/CT. Attempts

were made to image [^{99m}Tc]-DTPA in the paranasal sinus, intrathecal space, ventricles and cisterns.

(A) [^{99m}Tc]-DTPA SPECT/CT (30 min SPECT collection) coronal, horizontal, and sagittal sections showing some [^{99m}Tc]-DTPA in the intrathecal space (thoracic spine). Noise is high. (B) SPECT/CT focus on the kidneys showing renal clearance of [^{99m}Tc]-DTPA. (C) SPECT/CT focus on the cisterns, ventricles, and paranasal sinus. Intrathecal [^{99m}Tc]-DTPA activity is not resolvable in these structures. Noise is high. (D) SPECT/CT focus on the bladder showing renal clearance. (E) SPECT/CT horizontal and sagittal projections of (A) and (B) showing signal in spine, bladder, and kidneys, where signal is barely above background (see supporting video S8). An Inveon SPECT/CT and 2 rats were used in intrathecal [^{99m}Tc]-DTPA experiments. Our single pinhole Inveon SPECT/CT may be insufficient in resolving 100 μCi quantities of [^{99m}Tc]-DTPA. More advanced multi-pinhole SPECT systems may produce superior images. Dynamic imaging (see supporting video S1 and S2) with 100 μCi of [^{99m}Tc]-DTPA activity is not possible on the Inveon SPECT/CT.

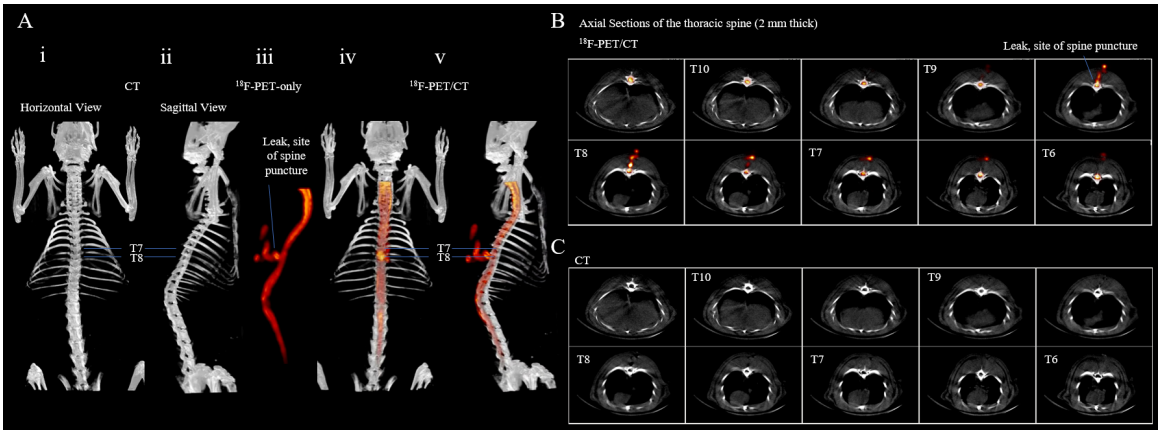

Supporting figure S15. Trauma model #2. Spinal cord puncture REPLICATE NUMBER 2. The thoracic spine between T7 and T8 is lacerated with a single blade of a Skylar 987810 Vannas scissors. [$^{18/19}$F]-**2** is intrathecally injected, post-trauma, and used to identify the site of spinal cord puncture that is not visible by (i) horizontal and (ii) sagittal CT. PET/CT imaging of intrathecal [$^{18/19}$F]-**2** show the leak site between T7 and T8 in (iii) maximum intensity projection PET (red), (iv) horizontal PET/CT, and (v) sagittal PET/CT. (B) Superior to inferior, axial 2.5 mm PET/CT sections of intrathecal [$^{18/19}$F]-**2** in the thoracic spine show a clear leak between T7 and T8. (C) The PET overlay is removed. Spinal defects that would indicate the site of puncture are not observable in CT. The puncture site is not obvious in CT.

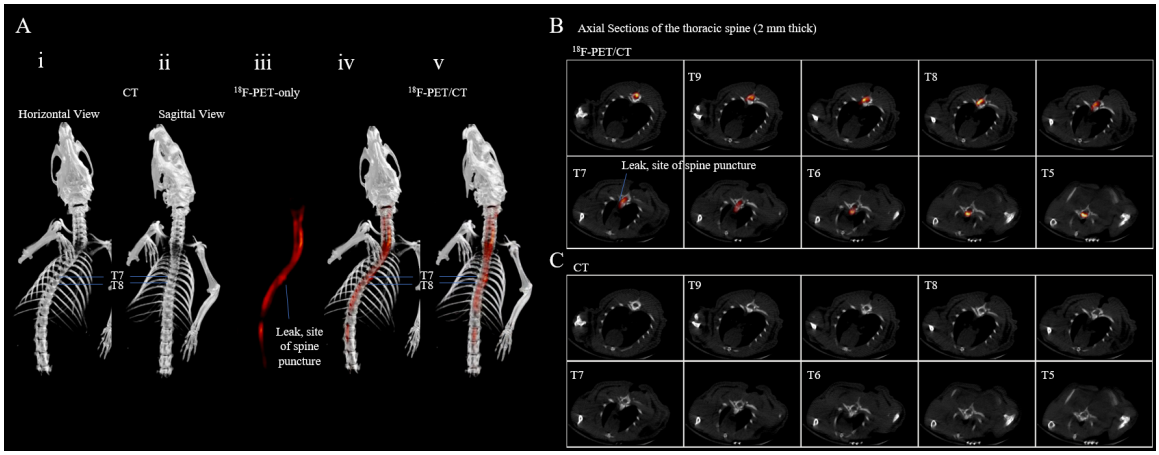

Supporting figure S16. Trauma model #2. Spinal cord puncture REPLICATE NUMBER 3. The thoracic spine between T7 and T8 is penetrated with a 25G needle (0.5144 ±0.0064 mm). [$^{18/19}$F]-**2** is intrathecally injected, post-trauma, and used to identify the site of spinal cord puncture that is not visible by (i) horizontal and (ii) sagittal CT. PET/CT imaging of intrathecal [$^{18/19}$F]-**2** show the leak site between T7 and T8 in (iii) maximum intensity projection PET (red), (iv) horizontal PET/CT, and (v) sagittal PET/CT. (B) Superior to inferior, axial 2.5 mm PET/CT sections of intrathecal [$^{18/19}$F]-**2** in the thoracic spine show a clear leak between T7 and T8. (C) The PET overlay is removed. Spinal defects that would indicate the site of puncture are not observable in CT. The puncture site is not obvious in CT.

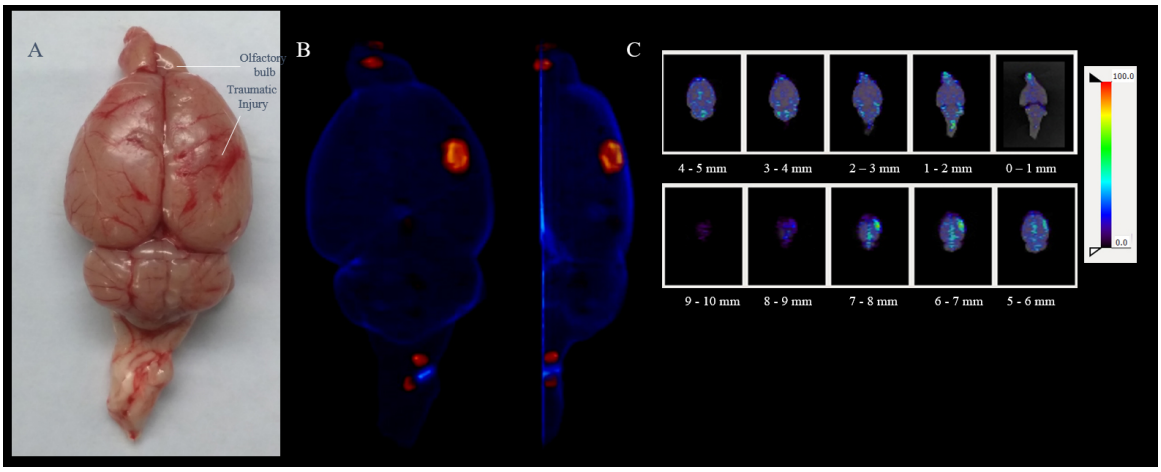

Supporting figure S17. Trauma model #3. Cryolesion-induced traumatic brain injury REPLICATE NUMBER 2. (A) Ex vivo bright field image showing superficial hemorrhage on the right neocortex. This is corroborated by (B) PET (red)/CT (blue) imaging of [$^{18/19}$F]-**2** that is injected intrathecally, 30 min post-cryolesion. (C) Horizontal 1 mm PET (NIH color table) /CT (grey) sections of (B) the brain showing signal at the site of the TBI and in the 3rd/4th ventricles and cisterna magna. 1 mm sections run inferior (+0 mm) to superior (+10 mm).